Geochemistry Geophysics Geosystems G3
AN ELECTRONIC JOURNAL OF THE EARTH SCIENCES
Published by AGU and the Geochemical Society

Research Letter
Volume 9, Number 11
22 November 2008
Q11009, doi:10.1029/2008GC002231
ISSN: 1525-2027

A physical model for widespread near-surface and fault zone damage induced by earthquakes

Shuo Ma

Department of Geological Sciences, San Diego State University, 5500 Campanile Drive, San Diego, California 92182-1020, USA (sma@geology.sdsu.edu)

[1] I present a rigorous unifying interpretation of the well-documented widespread near-surface and fault zone damage induced by earthquakes by simulating three-dimensional dynamic rupture propagation on a vertical strike-slip fault. Stresses in the crust are depth-dependent and material response is governed by the Drucker-Prager yielding criterion. I show that material yielding induced by seismic waves under the low confining pressure causes widespread near-surface damage. Because the confining pressure increases with depth, the yielding zone at depth is narrowly confined near the fault, but its thickness broadens dramatically near the surface, forming a "flower-like" damage zone. The fault zone damage at depth is induced by large dynamic stresses associated with the rupture front, while is induced by strong seismic waves ahead of the rupture front near the Earth's surface. These results have important implications for the formation and evolution of fault zones and possibly for the dynamic triggering of earthquakes as well.

Components: 4448 words, 6 figures.

Keywords: near-surface damage; fault zone damage; dynamic rupture.

Index Terms: 7209 Seismology: Earthquake dynamics (1242); 7215 Seismology: Earthquake source observations (1240); 7260 Seismology: Theory.

Received 5 September 2008; **Revised** 23 September 2008; **Accepted** 1 October 2008; **Published** 22 November 2008.

Ma, S. (2008), A physical model for widespread near-surface and fault zone damage induced by earthquakes, *Geochem. Geophys. Geosyst.*, *9*, Q11009, doi:10.1029/2008GC002231.

1. Introduction

[2] Seismic observations indicate that material velocities at shallow depths decrease over a large area after large earthquakes [*Poupinet et al.*, 1984; *Dodge and Beroza*, 1997; *Schaff and Beroza*, 2004; *Rubinstein and Beroza*, 2004, 2005; *Rubinstein et al.*, 2007; *Wegler and Sens-Schronfelder*, 2007]. The reductions are widespread and occur at distances of up to several source dimensions. A persistent low-velocity fault zone has also been documented extensively from seismic [e.g., *Li et al.*, 1990, 1998; *Vidale and Li*, 2003; *Li and Malin*, 2008; *Peng et al.*, 2003; *Ben-Zion et al.*, 2003; *Peng and Ben-Zion*, 2006] and geodetic [*Fialko et al.*, 2002] observations, in which the velocity drops further after large earthquakes.

[3] Dynamic stresses carried by seismic waves in the near surface [*Poupinet et al.*, 1984; *Dodge and Beroza*, 1997; *Schaff and Beroza*, 2004; *Rubinstein and Beroza*, 2004, 2005; *Rubinstein et al.*, 2007] or accompanying rupture in the fault zone [*Li et al.*, 1990, 1998; *Vidale and Li*, 2003; *Li and Malin*, 2008; *Peng et al.*, 2003; *Ben-Zion et al.*, 2003; *Peng and Ben-Zion*, 2006] are thought to create these velocity reductions by causing material dam-

age. However, a rigorous physical interpretation as to why modest dynamic stresses can cause widespread near-surface damage, and why fault damage zones form, is lacking.

[4] Inelastic material response immediately adjacent to the fault provides a natural way to understand the fault zone damage induced by earthquakes. Although it has long been recognized that material can behave inelastically in response to strong shaking [e.g., *Kramer*, 1996], it was only recently that seismologists began to consider the inelastic material response off the fault and its importance to dynamic earthquake simulations [*Yamashita*, 2000; *Dalguer et al.*, 2003a; 2003b; *Andrews*, 2005; *Ben-Zion and Shi*, 2005; *Ando and Yamashita*, 2007; *Andrews et al.*, 2007; *Duan*, 2008a, 2008b; *Templeton and Rice*, 2008; *Viesca et al.*, 2008]. Here I construct what is, to my knowledge, the first three-dimensional (3-D) numerical simulation of dynamic rupture process incorporating a yielding criterion in the volume. I show that the 3-D nature of the fault, along with depth-dependent stress conditions in the crust, gives rise not only to the commonly observed "flower-like" damage zone near the fault [e.g., *Ben-Zion et al.*, 2003; *Rockwell and Ben-Zion*, 2007] but also to the widespread near-surface damage due to seismic waves.

2. Model

[5] I consider a vertical right-lateral strike-slip fault in a homogeneous half-space (Figure 1a). The material properties are 6000 m/s (P wave speed), 3464 m/s (S wave speed), and 2670 kg/m^3 (density). The fault extends 15 km vertically, and the hypocenter is 7.5 km deep. The fault is assumed sufficiently long such that the simulated rupture never reaches the fault edges along strike. The normal stresses in the medium are set to the lithostatic overburden minus the hydrostatic pore pressure, i.e., $\sigma_{xx} = \sigma_{yy} = \sigma_{zz} = -16.37$ MPa/km (stresses are positive in tension), and the shear stresses are chosen $\sigma_{xy} = -6.55$ MPa/km and $\sigma_{xz} = \sigma_{yx} = 0$, such that the ratio of initial shear stress and normal stress on the fault is 0.4. I rupture the fault dynamically using a widely used slip-weakening friction law [*Ida*, 1972] to describe the evolution of the shear stress on fault with slip, assuming the static and dynamic frictional coefficient, and the critical slip-weakening distance on the fault to be 0.6, 0.3, and 0.4 m, respectively. The stress conditions on the fault are illustrated in Figure 1b. The dynamic stress drop (initial shear stress minus the dynamic frictional stress) without normal stress change on the fault increases linearly with depth. I taper the dynamic frictional stress at 12–15 km depth to avoid an artificial, abrupt stopping of the rupture.

[6] In the simulation, I allow yielding to occur whenever the stress state violates a pressure-dependent Drucker-Prager yielding criterion [*Drucker and Prager*, 1952], which states

$$\begin{gathered}\tau_v = \sqrt{0.5 s_{ij} s_{ij}}, \\ \tau_v^y = -\sigma_{kk}/3 \sin\phi + c\cos\phi, \text{ and} \\ \tau_v \le \tau_v^y,\end{gathered} \tag{1}$$

where τ_v is a measure of the shear stress in the 3-D stress state, s_{ij} is the deviatoric stress, c is the cohesion, φ is the internal frictional angle, τ_v^y is the yield stress, and the summation over repeated indices is assumed. This yielding criterion is a smoother version of the Mohr–Coulomb yielding criterion and has the important property that the yield stress τ_v^y depends on the mean normal stress $\sigma_{kk}/3$, which has long been recognized as an inherent property of rocks and soils.

[7] I define a scalar quantity η to evaluate the accumulated material damage due to the plastic yielding, which is given by

$$\begin{gathered}\eta(t) = \int_0^t d\eta, \\ d\eta = \sqrt{0.5\left(d\varepsilon_{ij}^p - d\varepsilon_{kk}^p/3\right)\left(d\varepsilon_{ij}^p - d\varepsilon_{kk}^p/3\right)},\end{gathered} \tag{2}$$

where $d\varepsilon_{ij}^p$ is the plastic strain increment at one time step. The damage η is identical to the scalar magnitude of plastic strain $\varepsilon^p = \sqrt{0.5\left(\varepsilon_{ij}^p - \varepsilon_{kk}^p/3\right)\left(\varepsilon_{ij}^p - \varepsilon_{kk}^p/3\right)}$ if plastic strain components have constant ratios as they change with time, which is not the case near the Earth's surface. The quantity η is a better measure of the material damage due to yielding than the plastic strain ε^p because it does not decrease with time. For simplicity, the material is assumed cohesionless and tan $\varphi = 0.75$, which is larger than the static frictional coefficient (0.6) so that the fault represents a plane of weakness.

[8] Both the dynamic rupture propagation and the wave propagation are modeled using a finite element approach [*Ma and Liu*, 2006; *Ma et al.*, 2008], which has tremendous computational benefits in handling nonlinear material constitutive laws. A 50 km × 60 km × 25 km domain is discretized with a uniform grid of 50 m eight-node

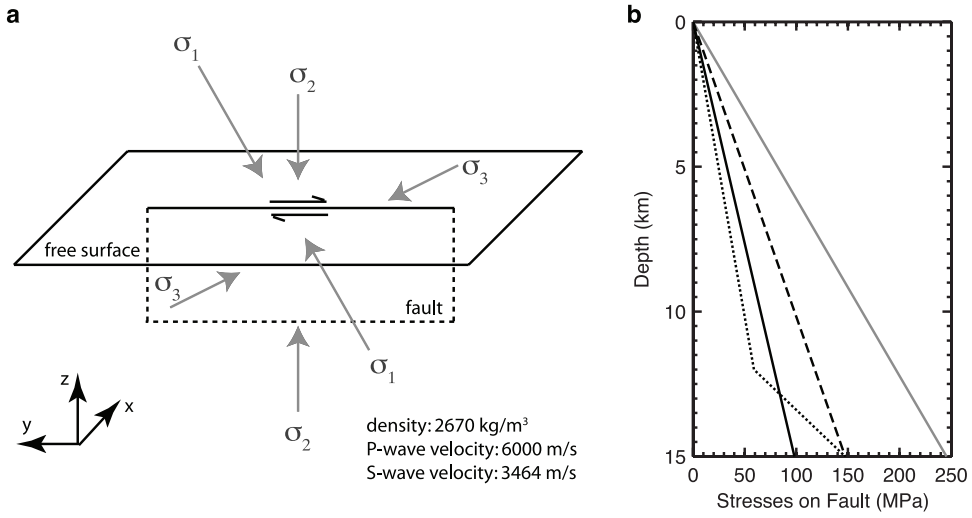

Figure 1. (a) Schematic of a vertical right-lateral strike-slip fault in a homogeneous half-space. Arrows show the three principal stresses for a strike-slip faulting environment. In the simulation, the chosen stress state implies that the most compressive principle stress σ_1 is 45° with respect to the fault. The coordinate system is shown on the lower left (the x and y axes are normal and parallel to the fault, respectively, and the z axis is vertical). (b) The depth-dependent stresses on the fault: normal stress σ_{xx} (gray solid line), shear stress σ_{xy} (black solid line), shear strength (dashed line), and dynamic frictional stress (dotted line). A linear taper is used for the dynamic frictional stress between 12 km and 15 km to avoid abrupt stopping of rupture at depth.

cubic elements, resulting in 600 million elements. An absorbing boundary condition is applied on all the boundaries except the free surface, in order to minimize spurious wave reflections. The time step is 0.008 s. The implementation of the plastic yielding in 3-D is a straightforward extension of the scheme of *Andrews* [2005], assuming no plastic volumetric deformation. Note that this implies $d\varepsilon^P_{kk} = 0$ in equation (2).

[9] The rupture is nucleated by forcing it to propagate at 2000 m/s until the rupture propagation becomes self-sustaining, which happens after about 2 s (Figure 2). The slip velocity is higher at depth than near the surface due to the linearly increasing dynamic stress drop with depth. Damage off the fault is clearly seen starting at about 1.2 s on the extensional side of the fault; however, when the rupture approaches the surface, the damage extends to the compressional side as well. The asymmetry in damage distribution across the fault induces normal stress changes on the fault [*Andrews*, 2005].

[10] Slices of accumulated damage distribution at different depths at 6 s are shown in Figures 3a–3f. The distributions are all antisymmetric with respect to the center of the fault. At depths (1.025–7.525 km), the damage distribution has a triangular shape, which is similar to results in two dimensions [e.g., *Andrews*, 2005]. The damage only occurs in the extensional side of the fault because of the decrease in the mean normal stress amplitude by the rupture front. Near the hypocentral depth the damage extends only about 350 m wide (Figure 3f). However, the width increases as it nears the surface. At 0.525 km depth, the damage starts to extend into the compressional side of the fault. At 25 m depth (the shallowest depth where the damage is defined in the model), the damage spreads over nearly a 1600 km^2 area surrounding the fault, which would be manifest in the Earth as widespread seismic wave velocity reductions [*Poupinet et al.*, 1984; *Dodge and Beroza*, 1997; *Schaff and Beroza*, 2004; *Rubinstein and Beroza*, 2004, 2005; *Rubinstein et al.*, 2007; *Wegler and Sens-Schronfelder*, 2007]. The strong asymmetry of damage zone at depth is also consistent with the observation in the Parkfield section of the San Andreas fault using fault zone trapped waves [*Li et al.*, 2006, 2007].

[11] Cross sections of the damage distribution clearly illustrate its depth dependence. The fault damage zone broadens dramatically as it approaches the surface. Such distributions resemble the "flower-like" fault zone structures inferred from seismic [e.g., *Ben-Zion et al.*, 2003] and geologic [e.g., *Sylvester*, 1988; *Rockwell and Ben-Zion*, 2007] studies of fault zones. Near the centerline

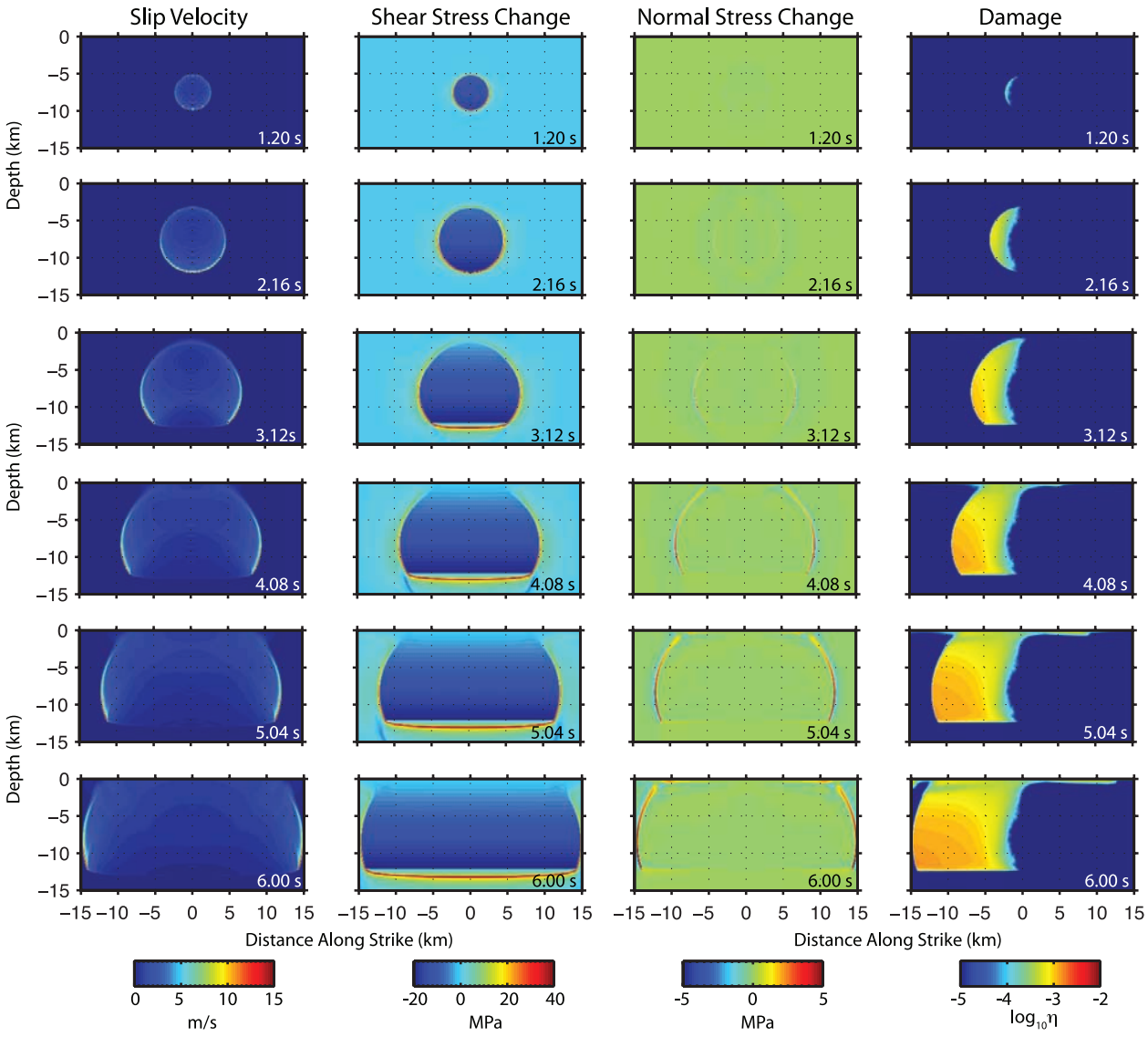

Figure 2. Snapshots of slip velocity, shear stress and normal stress variations of the dynamic rupture are mapped on the fault. Snapshots of the damage η (see definition in equation (2)) on a parallel plane 25 m off the fault are also mapped. Both the slip velocity and shear stress are along-strike component. The extensional side of the fault corresponds to negative distances along strike. The rupture is nucleated by forcing it to propagate radially at 2000 m/s starting from the hypocenter (7.5 km deep), and then starts to propagate spontaneously at a higher velocity after ~2 s. The larger slip velocity at depth is due to the linearly increasing stress drop with depth prescribed in the model. The damage only occurs in the extensional side of the fault at depth, but extends to the compressional side of the fault near the surface. The asymmetry of the damage across the fault causes the normal stress variation on the fault.

of the fault (Figure 3g), a nearly symmetric distribution of damage is seen across the fault. As the distance to the centerline increases, damage occurs mostly on the extensional side of the fault (Figures 3h–3m). The damage on the compressional side occurs only very near the surface (upper 1 km). Damage shown in Figures 3n–3p is entirely caused by the seismic waves radiated from the fault ahead of the rupture front. The damage zone at depth is narrowly confined near the fault due to the large confining pressure (Figure S1).[1]

[12] Time histories at three representative sites at 25 m depth (half element size below the surface) illustrate why and when the damage occurs

[1]Auxiliary materials are available in the HTML. doi:10.1029/2008GC002231.

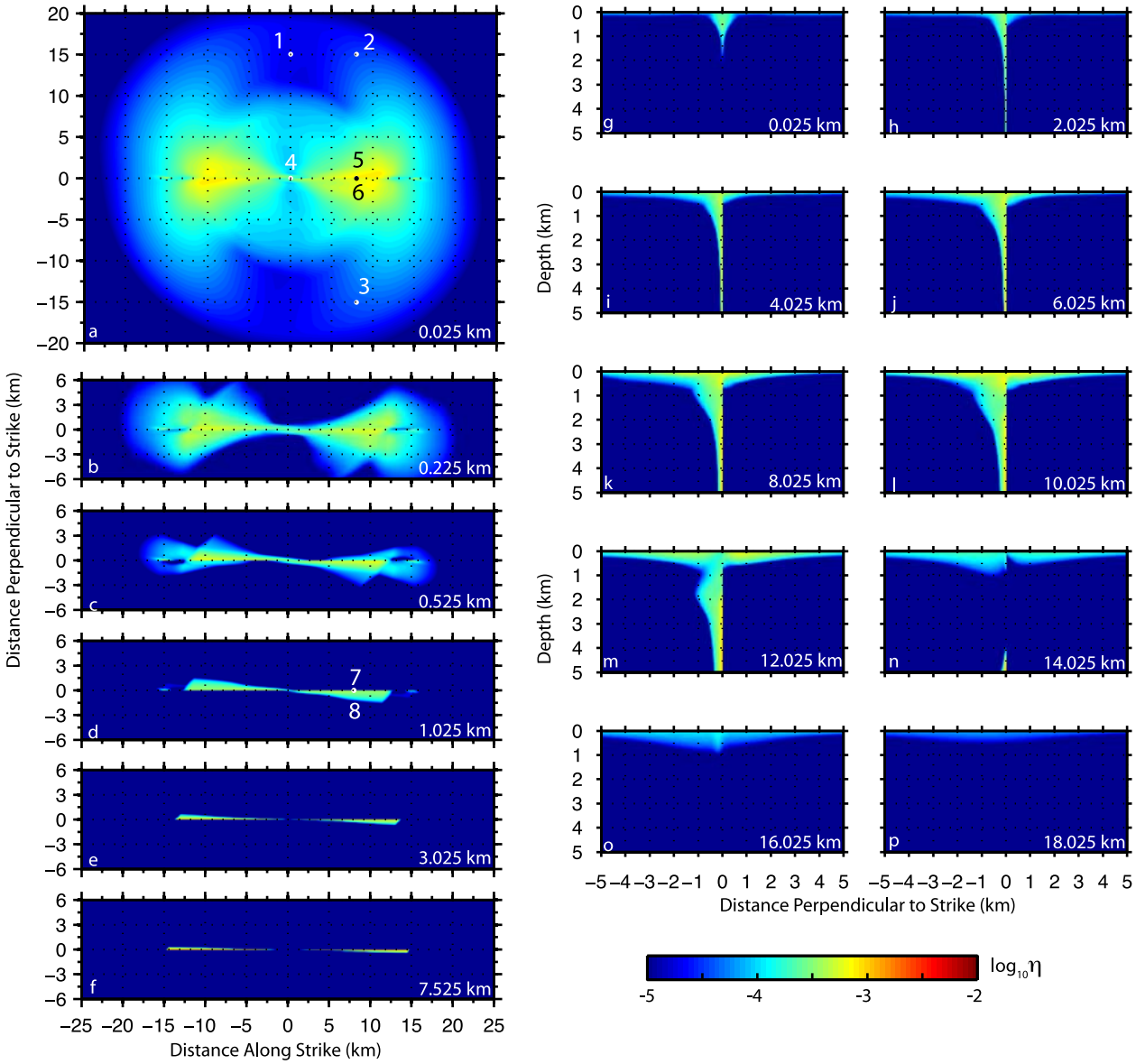

Figure 3. Distribution of damage η (see definition in equation (2)) at 6 s (a–f) at depths and at (g–p) cross sections perpendicular to the fault. Note that the scale is logarithmic. The depth or the distance along strike for each cross section is shown in each figure. The triangular shape of damage at depths is very similar to results in two dimensions. Owing to the high confining pressure, the damage occurs only on the extensional side of the fault at depth. However, at shallow depth, the damage occurs on both sides of the fault because of the small confining pressure. The damage at 0.025 km depth spreads over a very large area, corresponding to the widespread seismic wave velocity reductions. The thickness of damage zone broadens dramatically as it nears the surface, which gives rise to a "flower-like" damage zone near the fault. The dots denote eight sites where the time histories are plotted in Figures 4–5. Locations of the sites are site 1 (0.025, 15.025, −0.025); site 2 (8.025, 15.025, −0.025); site 3 (8.025, −15.025, −0.025); site 4 (0.025, 0.025, −0.025); site 5 (8.025, 0.025, −0.025); site 6 (8.025, −0.025, −0.025); site 7 (8.025, 0.025, −1.025); site 8 (8.025, −0.025, −1.025), where each number in the bracket denotes the distance along strike from the epicenter and perpendicular to strike and depth, respectively, and the unit is in kilometers.

(Figure 4). At this depth, the mean normal stress is 0.4 MPa, and equation (1) predicts that the yield stress is only ~0.25 MPa when the cohesion is zero. All 3 sites are located 15.025 km off the fault. Site 1 is 25 m off the antiplane direction, where only SH waves and almost no change in the mean normal stress are expected. The damage at this site is clearly induced by the amplitude increase of shear stress s_{xy} corresponding to arrivals of SH waves from the fault. Sites 2 and 3 are located

where combined effects of *P* and *S* waves cause the mean normal stress change. Again it is seen that due to the low confining pressure, the arrival of strong seismic waves causes the occurrence of damage, which is delayed at site 2 (compressional regime) relative to site 3 (the extensional regime).

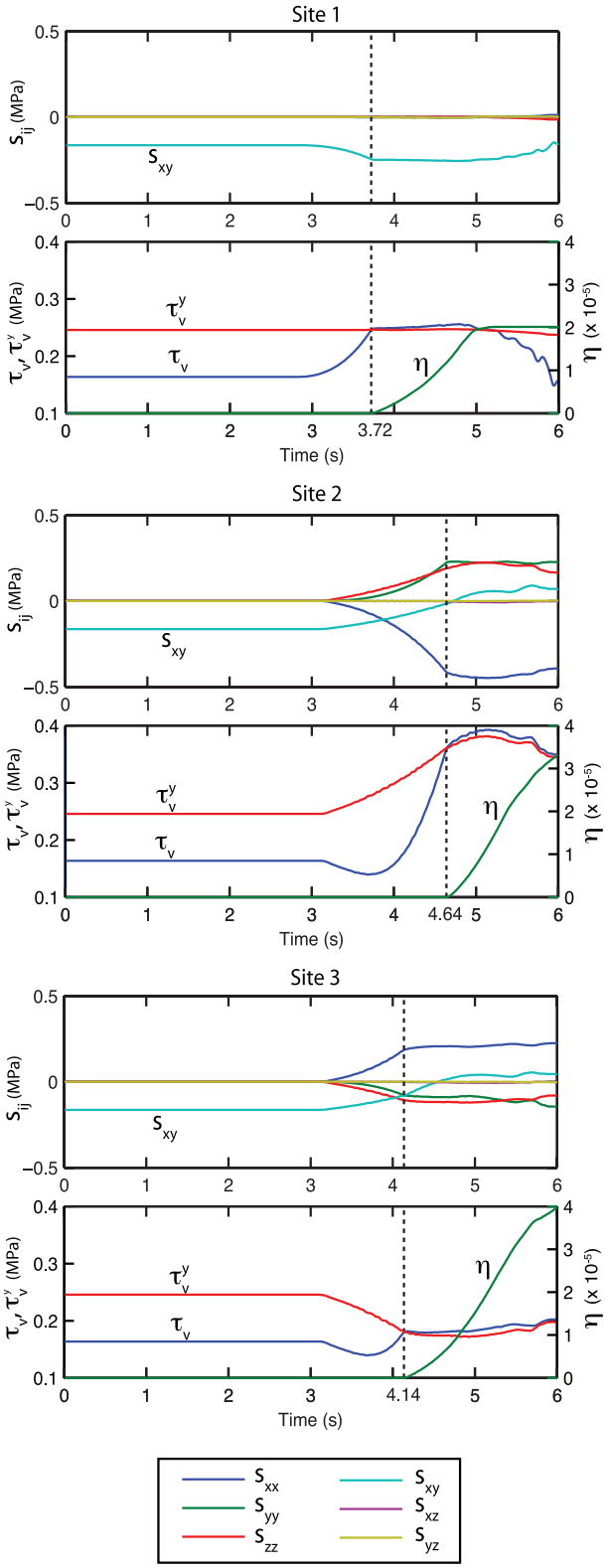

Figure 4. Plots of time histories of deviatoric stresses, the shear stress τ_v and yield stress τ_v^y (see definition in equation (1)), and damage η (see definition in equation (2)) at 3 sites (locations shown in Figure 3). The legend for the deviatoric stresses is shown at the bottom. The yield stress τ_v^y given by the yielding criterion is proportional to the mean normal stress. Site 1 is located near the antiplane direction, where there is little mean normal stress variation. Sites 2 and 3 are located in the compressional and extensional sides of the fault, respectively. The dashed line marks the initiation of the damage, which is induced by the dynamic stress carried by seismic waves under the low confining pressure. Sometimes the stress τ_v exceeds the yield stress τ_v^y, which is due to the viscoplasticity relaxation scheme [*Andrews*, 2005] used to relax the stresses smoothly back to the yield surface.

[13] Time histories at sites 4–8 show the behavior at distances very close to the fault (Figure 5). All the sites are 25 m off the fault. At site 4 (25 m off the antiplane direction), the shear stress s_{xy} first decreases its amplitude and the damage occurs when its amplitude increases in the opposite direction (2.44 s), well ahead of the arrival of the rupture front (3.13 s). After the rupture front passes, damage increases further, but there is little change in the mean normal stress. Sites 5 and 6 are 8.025 km along strike. Because they are only 25 m off the fault, large SH waves are expected. The occurrence of damage again coincides with the arrival of SH waves well ahead of the rupture front. At these two sites, the damage occurs simultaneously (induced by the same SH waves); but the amplitude of damage at site 5 (the compressional regime) is smaller than site 6 (the extensional regime), as a result of the differences in the rupture-induced mean normal stress changes on the different sides of the fault. At slightly greater depths (sites 7 and 8), it is a different story, however, because the slightly higher confining pressure allows damage induced by the rupture front in the extensional regime only.

3. Discussion and Conclusions

[14] Dynamic stresses associated with the seismic waves or the rupture front play the key role in plastic yielding of the material in the model. The correlation of the damage at 25 m depth with the peak ground velocity (Figure 6) supports this point. It is also consistent with the observation that main shock-induced velocity reductions are most

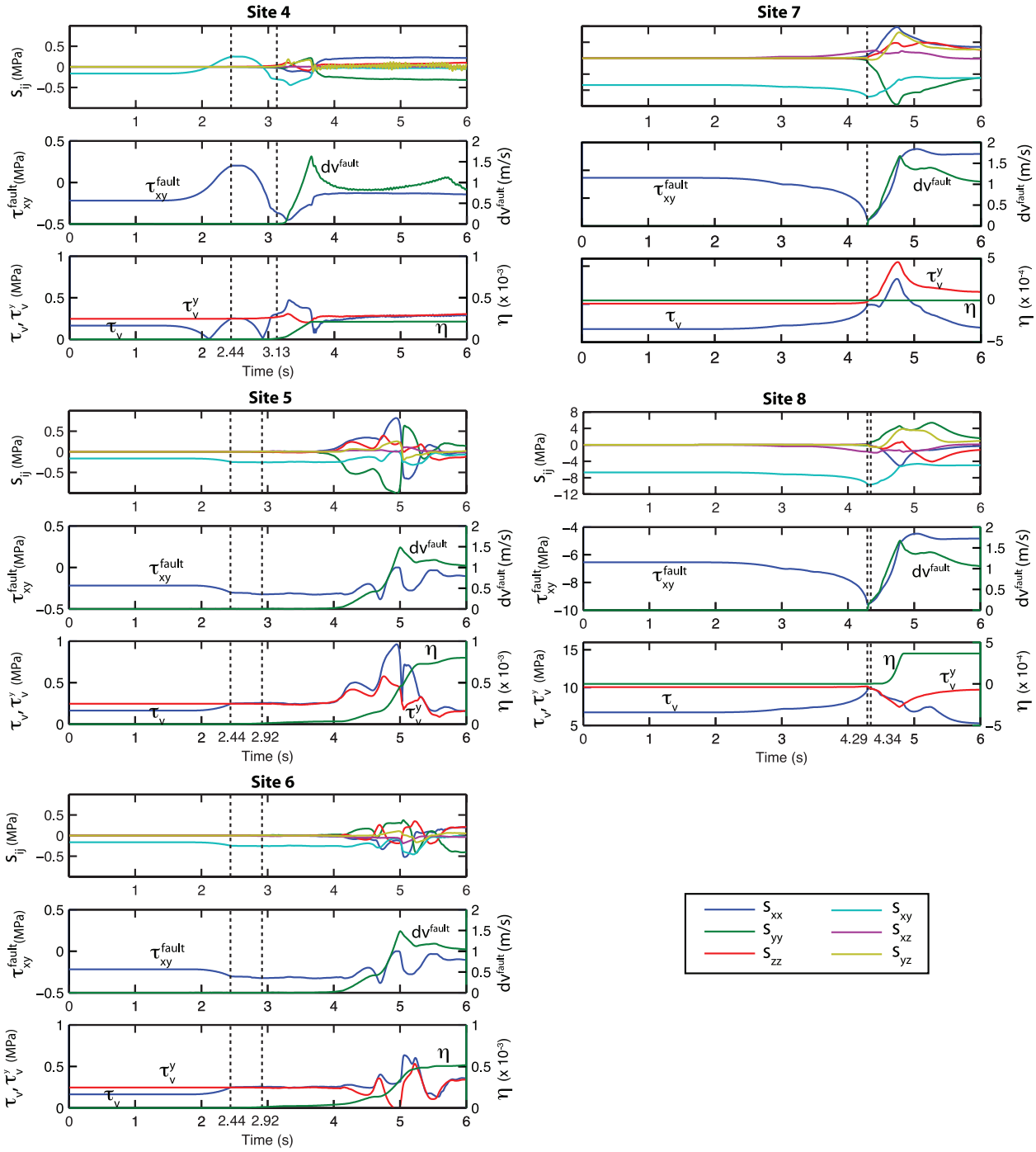

Figure 5. Similar to Figure 4 except for sites 4–8. Time histories of shear stress τ_{xy}^{fault} and slip velocity dv^{fault} (along-strike component) at the nearest point on the fault to each site are also plotted. The dashed line marks the initiation of the damage or the slip. At 25 km depth (sites 4–6) the damage is induced by seismic waves ahead of the rupture front. See text for details. At 1.025 km depth (sites 7 and 8), the damage is induced by the dynamic stress carried by the rupture front in the extensional side of the fault only, while there is no damage on the compressional side of the fault. The differences are due to the higher confining pressure at depth.

strongly correlated with peak ground velocity [e.g., *Dodge and Beroza*, 1997; *Schaff and Beroza*, 2004; *Rubinstein and Beroza*, 2004, 2005; *Rubinstein et al.*, 2007].

[15] This simple physical model provides a unifying physical interpretation of the widespread near-surface damage and the flower-like fault damage zone at shallow depths and also predicts that the

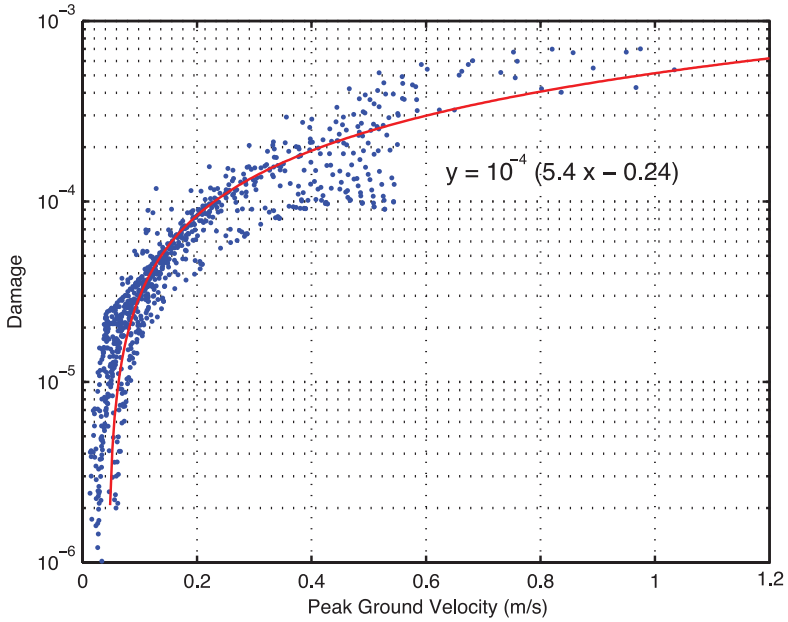

Figure 6. Plot of damage (see definition in equation (2)) as a function of peak ground velocity (PGV) for the points at 25 m depth (the shallowest depth where the damage ç is defined) in the simulation. The points are sampled every 1 km over the area (40 km × 50 km) shown in Figure 3a with points within 1 km of the fault or of the damage amplitude smaller than 10^{-6} removed. The PGV is chosen as the larger of the two horizontal velocity components' amplitude because the vertical velocity amplitude is much smaller. The data are fit by a linear relation (solid line). The damage clearly increases with the PGV in the simulation.

damage at depths is narrowly confined near the fault.

[16] Although pore fluids and material heterogeneity in the crust might also play a role in the distribution of near-surface and fault zone damage, this simple physical model demonstrates an important effect caused by the overburden pressure. The zero cohesion assumed in the simulation is clearly an end-member case. The cohesion will certainly limit the spatial extent of the damage to a certain degree; however, the pattern of the damage distribution is not likely to change as the yielding occurs more easily near the surface due to a smaller overburden pressure. This point, however, will need to be confirmed by future studies.

[17] The damage pattern reported here is due to a single seismic event. Repeated damage during the many seismic events that occur over geologic time contributes to the formation and evolution of fault zone structures [*Sylvester*, 1988; *Ben-Zion and Sammis*, 2003]. Shaking-induced damage may also play an important role in the dynamic triggering of earthquakes [*Johnson and Jia*, 2005].

Acknowledgments

[18] I am grateful to Joe Andrews and Yonggang Li for insightful reviews and Greg Beroza and Ruth Harris for numerous helpful comments. This work is partly supported by the U.S. Geological Survey (USGS), Department of Interior, under USGS award 08HQGR0013. The views and conclusions contained in this document are those of the author and should not be interpreted as necessarily representing the official policies, either expressed or implied, of the U.S. Government.

References

Ando, R., and T. Yamashita (2007), Effects of mesoscopic-scale fault structure on dynamic earthquake ruptures: Dynamic formation of geometrical complexity of earthquake faults, *J. Geophys. Res.*, *112*, B09303, doi:10.1029/2006JB004612.

Andrews, D. J. (2005), Rupture dynamics with energy loss outside the slip zone, *J. Geophys. Res.*, *110*, B01307, doi:10.1029/2004JB003191.

Andrews, D. J., T. C. Hanks, and J. W. Whitney (2007), Physical limits on ground motion at Yucca Mountain, *Bull. Seismol. Soc. Am.*, *97*, 1771–1792, doi:10.1785/0120070014.

Ben-Zion, Y., and C. G. Sammis (2003), Characterization of fault zones, *Pure Appl. Geophys.*, *160*, 677–715, doi:10.1007/PL00012554.

Ben-Zion, Y., and Z. Shi (2005), Dynamic rupture on a material interface with spontaneous generation of plastic strain in the bulk, *Earth Planet. Sci. Lett.*, *236*, 486–496, doi:10.1016/j.epsl.2005.03.025.

Ben-Zion, Y., Z. Peng, D. Okaya, L. Seeber, L. G. Armbruster, N. Ozer, A. J. Michael, S. Baris, and M. Aktar (2003), A shallow fault zone structure illuminated by trapped waves in the Karadere-Duzce branch of the North Anatolian fault, western Turkey, Geophys, *J. Int.*, *152*, 699–717, doi:10.1046/j.1365-246X.2003.01870.x.

Dalguer, L. A., K. Irikura, and J. D. Riera (2003a), Simulation of tensile crack generation by three-dimensional dynamic shear rupture propagation during an earthquake, *J. Geophys. Res.*, *108*(B3), 2144, doi:10.1029/2001JB001738.

Dalguer, L. A., K. Irikura, and J. D. Riera (2003b), Generation of new cracks accompanied by the dynamic shear rupture propagation of the 2000 Tottori (Japan) earthquake, *Bull. Seismol. Soc. Am.*, *93*, 2236–2262, doi:10.1785/0120020171.

Dodge, D. A., and G. C. Beroza (1997), Source array analysis of coda waves near the 1989 Loma Prieta, California, mainshock: Implications for the mechanism of coseismic velocity changes, *J. Geophys. Res.*, *102*(B11), 24,437–24,458, doi:10.1029/97JB02024.

Drucker, D. C., and W. Prager (1952), Soil mechanics and plastic analysis or limit design, *Q. Appl. Math.*, *10*, 157–165.

Duan, B. (2008a), Effects of low-velocity fault zones on dynamic ruptures with nonelastic off-fault response, *Geophys. Res. Lett.*, *35*, L04307, doi:10.1029/2008GL033171.

Duan, B. (2008b), Asymmetric off-fault damage generated by bilateral ruptures along a bimaterial interface, *Geophys. Res. Lett.*, *35*, L14306, doi:10.1029/2008GL034797.

Fialko, Y., D. Sandwell, D. Agnew, M. Simons, P. Shearer, and B. Minster (2002), Deformation on nearby faults induced by the 1999 Hector Mine earthquake, *Science*, *297*, 1858–1862, doi:10.1126/science.1074671.

Ida, Y. (1972), Cohesive force across the tip of a longitudinal shear crack and Griffith's specific surface energy, *J. Geophys. Res.*, *77*, 3796–3805, doi:10.1029/JB077i020p03796.

Johnson, A. A., and X. Jia (2005), Nonlinear dynamics, granular media and dynamic earthquake triggering, *Nature*, *437*, 871–874, doi:10.1038/nature04015.

Kramer, S. L. (1996), *Geotechnical Earthquake Engineering*, Prentice Hall, Upper Saddle River, N. J.

Li, Y.-G., and P. E. Malin (2008), San Andreas Fault damage at SAFOD viewed with fault-guided waves, *Geophys. Res. Lett.*, *35*, L08304, doi:10.1029/2007GL032924.

Li, Y. G., P. C. Leary, K. Aki, and P. E. Malin (1990), Seismic trapped modes in the Oroville and San Andreas fault zones, *Science*, *249*, 763–766, doi:10.1126/science.249.4970.763.

Li, Y. G., J. E. Vidale, K. Aki, F. Xu, and T. Burdette (1998), Evidence of shallow fault zone strengthening after the 1992 M7.5 Lander, California, earthquake, *Science*, *279*, 217–219, doi:10.1126/science.279.5348.217.

Li, Y. G., P. Chen, E. S. Cochran, J. E. Vidale, and T. Burdette (2006), Seismic evidence for rock damage and healing on the San Andreas fault associated with the 2004 M6 Parkfield earthquake, Special issue for Parkfield M6 earthquake, *Bull. Seismol. Soc. Am.*, *96*(4), S1–S15.

Li, Y. G., P. Chen, E. S. Cochran, and J. E. Vidale (2007), Seismic velocity variations on the San Andreas Fault caused by the 2004 M6 Parkfield earthquake and their implications, *Earth Planets Space*, *59*, 21–31.

Ma, S., and P. Liu (2006), Modelling of the perfectly matched layer absorbing boundaries and intrinsic attenuation in explicit finite-element methods, *Bull. Seismol. Soc. Am.*, *96*, 1779–1794, doi:10.1785/0120050219.

Ma, S., S. Custodio, R. J. Archuleta, and P. Liu (2008), Dynamic modeling of the M_w 6.0 Parfield, California, earthquake, *J. Geophys. Res.*, *113*, B02301, doi:10.1029/2007JB005216.

Peng, Z., and Y. Ben-Zion (2006), Temporal changes of shallow seismic velocity around the Karadere-Duzce branch of the North Anatolian Fault and strong ground motion, *Pure Appl. Geophys.*, *163*, 567–599, doi:10.1007/s00024-005-0034-6.

Peng, Z., Y. Ben-Zion, A. J. Michael, and L. Zhu (2003), Quantitative analysis of seismic trapped waves in the rupture zone of the 1992 Landers, California earthquake: Evidence for a shallow trapping structure, *Geophys. J. Int.*, *155*, 1021–1041, doi:10.1111/j.1365-246X.2003.02109.x.

Poupinet, G., W. L. Ellsworth, and J. Frechet (1984), Monitoring velocity variations in the crust using earthquake doublets: An application to the Calaveras Fault California, *J. Geophys. Res.*, *89*, 5719–5731, doi:10.1029/JB089iB07p05719.

Rockwell, T. K., and Y. Ben-Zion (2007), High localization of primary slip zones in large earthquakes from paleoseismic trenches: Observations and implications for earthquake physics, *J. Geophys. Res.*, *112*, B10304, doi:10.1029/2006JB004764.

Rubinstein, J. L., and G. C. Beroza (2004), Evidence for widespread nonlinear strong ground motion in the Mw 6.9 Loma Prieta earthquake, *Bull. Seismol. Soc. Am.*, *94*, 1595–1608, doi:10.1785/012004009.

Rubinstein, J. L., and G. C. Beroza (2005), Depth constraints on nonlinear strong ground motion from the Parkfield earthquake, *Geophys. Res. Lett.*, *32*, L14313, doi:10.1029/2005GL023189.

Rubinstein, J. L., N. Uchida, and G. C. Beroza (2007), Seismic velocity reductions caused by the 2003 Tokachi-Oki earthquake, *J. Geophys. Res.*, *112*, B05315, doi:10.1029/2006JB004440.

Schaff, D. P., and G. C. Beroza (2004), Coseismic and postseismic velocity changes measured by repeating earthquakes, *J. Geophys. Res.*, *109*, B10302, doi:10.1029/2004JB003011.

Sylvester, A. G. (1988), Strike-slip faults, *Geol. Soc. Am. Bull.*, *100*, 1666–1703, doi:10.1130/0016-7606(1988)100<1666:SSF>2.3.CO;2.

Templeton, E. L., and J. R. Rice (2008), Off-fault plasticity and earthquake rupture dynamics, 1. Dry materials or neglect of fluid pressure changes, *J. Geophys. Res.*, *113*, B09306, doi:10.1029/2007JB005529.

Vidale, J. E., and Y.-G. Li (2003), Damage to the shallow Landers fault from the nearby Hector Mine earthquake, *Nature*, *421*, 524–526, doi:10.1038/nature01354.

Viesca, R. C., E. L. Templeton, and J. R. Rice (2008), Off-fault plasticity and earthquake rupture dynamics, 2. Case of saturated off-fault materials, *J. Geophys. Res.*, *113*, B09307, doi:10.1029/2007JB005530.

Wegler, U., and C. Sens-Schronfelder (2007), Fault zone monitoring with passive image interferometry, *Geophys. J. Int.*, *168*, 1029–1033, doi:10.1111/j.1365-246X.2006.03284.x.

Yamashita, T. (2000), Generation of microcracks by dynamic shear rupture and its effects on rupture growth and elastic wave radiation, *Geophys. J. Int.*, *143*, 395–406, doi:10.1046/j.1365-246X.2000.01238.x.